Ultrasound Scattering from a Rigid Sphere Using the Discontinuous Galerkin Method in the Time-Explicit Domain

D. Rubinetti[1] D. A. Weiss[1] E. Weingartner[2] M. Lenner[3]

[1]Institute of Thermal- and Fluid-Engineering, University of Applied Sciences and Arts Northwestern Switzerland
[2]Institute of Sensors and Electronics, University of Applied Sciences and Arts Northwestern Switzerland
[3]Corporate Research Center, ABB Switzerland Ltd.

Abstract

Ultrasound technology is deployed in a variety of scientific and engineering applications predominantly in liquid media. The use of ultrasound in gaseous environments has not yet reached the same level of maturity - especially in the context of industrial measurements. The present study focuses on fundamental investigation of propagation properties of airborne acoustic waves and their interaction with solids. For this purpose, the scattering behavior of ultrasonic waves from rigid spheres is examined. Four different sphere radii a are studied, being 0.001, 0.1, 1 and 100 times the wavelength λ. The geometry is a 2D-axisymmetric enclosure with the sphere placed in the center of the $z-axis$. The model is based on the *Convected Wave Equation, Time Explicit* interface which features the discontinuous Galerkin method to solve the set of linearized Euler equations due to its capability to handle large-distance propagation problems in a memory-efficient way. To verify the results, the simulations are compared with an analytical model for rigid scattering from a sphere. In addition, a mesh convergence assesment was performed. Analytical and numerical results show perfect agreement laying the groundwork for improved acoustic simulations that include loss mechanisms.

Keywords: Acoustics, Scattering, discontinuous Galerkin, Ultrasound

1 Introduction

In nature, ultrasound is a rare occurrence. Only a few animals use ultrasound to scan their surroundings or to transmit information, such as bats and whales. Nonetheless, ultrasound has become wide-spread and well-established in scientific and engineering applications. The application spectrum of ultrasound technology ranges from the harvesting of nanometer particles up to the stirring of molten metal (Rubinetti and Weiss, 2018a,b), including the capability of triggering a physical process in a non-intrusive and non-destructive fashion. As of today, ultrasound is a mature technique predominantly in liquid and solid media. In gaseous environments, ultrasound technology has not yet reached the same level of industrial importance.
In this study, the objective is to conceive a verifiable testcase for acoustic scattering in air from a rigid sphere. The novelty of this study is the use of the *Convected Wave Equation* (CWE) interface that is based on the discontinuous Galerkin (dG) method, which provides a memory-efficient approach for solving propagation problems of ultrasonic waves.

2 Physical Model

CWE is in principle an interface to model the propagation of ultrasound over large distances, *i.e.* distances large compared to the wavelength λ. However, this study tackles the challenging task to model acoustic scattering with CWE in the time-explicit domain.

2.1 Scattering regimes

When it comes to acoustic scattering, four different regimes exist as shown in Figure 1.

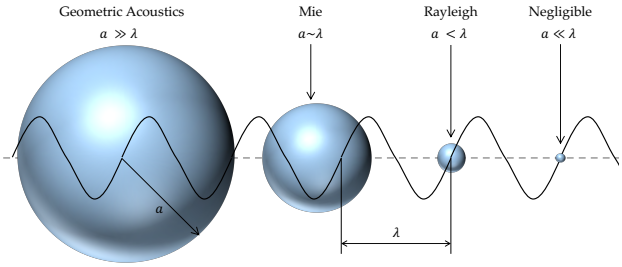

Figure 1. Schematic drawing of the range of validity for the four different scattering regimes, geometric acoustics, Mie, Rayleigh and negligible scattering.

Geometric acoustics, or ray acoustics, holds when the scattering obstacle is large compared to the wavelength. Mie scattering is the case when λ and the sphere radius a are comparable. In the Rayleigh regime $a < \lambda$ acoustic scattering is characterized by an elastic reflection of incoming waves while for smallest sphere the scattered pressure is vanishingly small.

2.2 Plane wave scattering

As benchmark model this study uses the case of acoustic scattering of a plane wave from a rigid sphere. Despite its simplicity, plane wave scattering continues to attract the attention of researchers (Adam, 2017). An important

parameter to characterize scattering phenomena is the dimensionless wave number ka

$$ka = \frac{2\pi}{\lambda}a \tag{1}$$

where $\lambda = c/f$ with $c = 343\ \mathrm{m\,s^{-1}}$ being the speed of sound in air and f being the frequency. Ultrasonic frequencies, as of interest in this work, start from 20 kHz and reach up to several Megahertz.

Mathematically, acoustic scattering of an incident plane wave from a rigid sphere is a well-studied problem (Weser et al., 2013, 2014). It has been thoroughly analyzed in the time-harmonic domain where the acoustic field variables oscillate sinusoidally in time. Figure 2 illustrates the system sketch in spherical coordinates with the incident plane wave

$$p_{inc}(r,\theta) = p_a \cdot e^{ikrcos(\theta)} \tag{2}$$

with p_a being the pressure amplitude of the incoming wave. Rigid scattering implies a Neumann-type boundary condition on ∂D such that

$$\frac{\partial p_{inc}}{\partial r} = -\frac{\partial p_{sc}}{\partial r} \tag{3}$$

where p_{sc} denotes the scattered pressure. Note that the boundary condition according to Equation (3) implies that all incoming acoustic energy is reflected by the boundary without any transmission or absorption by the sphere (*i.e.* *sound hard* boundary condition).

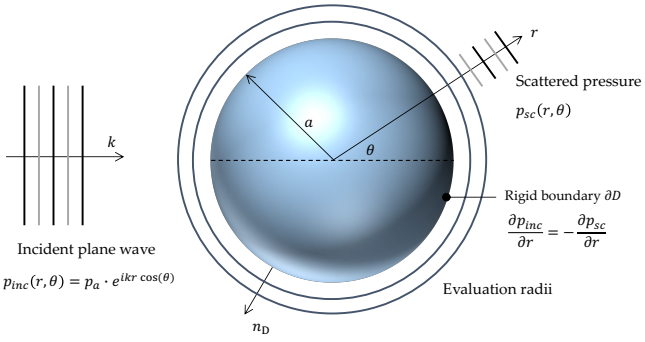

Figure 2. System sketch for the analytical description of acoustic scattering from a rigid sphere in spherical coordinates.

The CWE interface in COMSOL computes the acoustic variable in the time-explicit domain. To compare the time-harmonic analytical solution and the numerical solution a time-averaging or interpolation algorithm shall be applied.

2.3 Analytical model

The complex-valued analytical solution for the scattered pressure p_{sc} is given by (Ihlenburg, 2006)

$$p_{sc}(r,\theta) = -p_a \sum_{n=0}^{\infty} (2n+1) i^n h_n^{(1)}(kr) \frac{j_n'(ka)}{h_n'^{(1)}(ka)} P_n(\cos\theta). \tag{4}$$

The scattered pressure p_{sc} is described by an infinite series of spherical Hankel functions $h_n^{(1)}$, derivatives of spherical Bessel j_n' and Hankel functions $h_n'^{(1)}$ as well as Legendre Polynomials P_n. With p_{sc} being complex-valued, only its real part $\Re(p_{sc})$ is physically relevant to verify the numerical model. Figure 3 shows the radiation plot of the scattered pressure of a rigid sphere $\lambda = a$ at 50 kHz with an incident wave hitting the sphere at 180°.

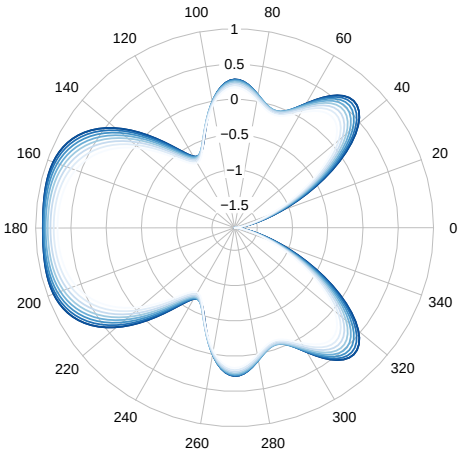

Figure 3. Radiation plot of a rigid sphere ($a = \lambda$) being hit by an incoming plane wave at 180° with a pressure amplitude $p_a = 1$ Pa. The different lines correspond to evaluation radii $a \leq r \leq 1.08a$.

The sphere size to wavelength ratio plays an important role in determining the intensity and directivity of the scattered pressure. Due to meshing considerations of the discontinuous Galerkin approach the numerical analysis is limited to the $a = \lambda$ case. To complete the study with further particle sizes and for verification purposes, Equation (4) for the scattered pressure is implemented into an analytical model coded in the open-source software R. Figure 4 shows the resulting radiation plots of the analytical model for further particle sizes a. With decreasing particle size the direction of sound diffraction becomes perpendicular (90°) to the direction of the incoming plane wave (at 180°). Larger particles diffract a notable fraction of the scattered acoustic pressure in backward direction, *i.e.* against the plane wave propagation direction.

3 Numerical Model

Within the *Acoustics* module several interfaces exist with predefined features to model acoustic scattering. This study uses the CWE interface instead which poses a novelty in modeling scattering phenomena with COMSOL

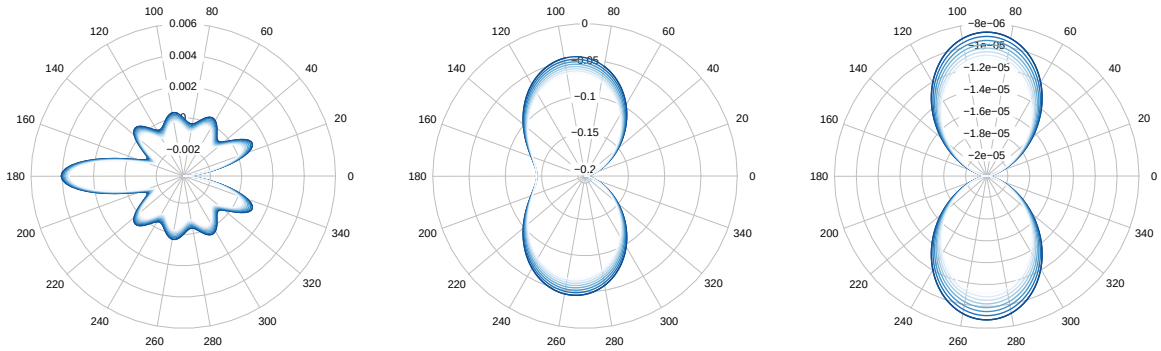

(a) $a = 100\lambda = 686$ mm **(b)** $a = 0.1\lambda = 0.68$ mm **(c)** $a = 0.001\lambda = 6.86$ µm

Figure 4. Results of the analytical model to visualize the directivity and intensity of the scattered pressure for various particle sizes. The incident plane wave with a pressure amplitude of $p_a = 1$ Pa hits the particle at 180° with a frequency of $f = 50$ kHz.

5.4. The reason for choosing CWE is to conceive a coherent modeling approach which allows the extension of the model for a broader range of applications (*e.g.* modeling background flow fields).

3.1 Governing equations

In the CWE interface the following set of equations is solved

Mass conservation

$$\frac{\partial \rho}{\partial t} + (\boldsymbol{u}_0 \cdot \nabla)\rho + (\boldsymbol{u} \cdot \nabla)\rho_0 + \rho(\nabla \cdot \boldsymbol{u}_0) + \rho_0(\nabla \cdot \boldsymbol{u}) = f_p \quad (5)$$

Momentum conservation

$$\frac{\partial \boldsymbol{u}}{\partial t} + (\boldsymbol{u}_0 \cdot \nabla)\boldsymbol{u} + (\boldsymbol{u} \cdot \nabla)\boldsymbol{u}_0 + \frac{1}{\rho_0}\nabla p - \frac{\rho}{{\rho_0}^2}\nabla p_0 = \boldsymbol{f}_v \quad (6)$$

Adiabatic equation of state

$$p = c^2 \rho. \quad (7)$$

ρ is the acoustic perturbation density, $\boldsymbol{u}_0$ the stationary background flow field velocity, ρ_0 the fluid density, $\boldsymbol{u}$ the acoustic velocity, f_p is the mass source or sink, p the acoustic pressure and p_0 the background pressure. The momentum equation features the source term $\boldsymbol{f}_v$. Since convective effects based on a stationary background field are omitted, flow field variables are disregarded which reduces the set of equations to the time-dependent wave-equation.

3.2 Setup and boundary conditions

The numerical analysis of acoustic scattering with CWE requires some preparatory work. In contrast to the previously described analytical model in a spherical coordinate system, the numerical model is based on a 2D-axisymmetric geometry which corresponds to cylindrical coordinates. Figure 5 shows the setup with computational domain Ω where the sphere size is magnified for illustration purposes. For the simulation we chose the condition $a = \lambda$, that is the sphere radius equals to the wavelength, which corresponds to 6.86 mm at 50 kHz in air. This particle size is purposeful to determine a suitable modeling approach. Such dimensions are spatially discretizable for a numerical solver which poses the basis to compare analytical and numerical results.

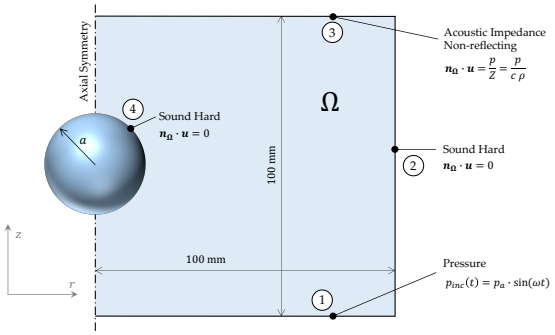

Figure 5. System sketch for the acoustic scattering numerical model with computational domain Ω and boundary conditions.

On the pressure boundary (1), at $t = 0$ s a pressure of 0 Pa is imposed, which demands for a Dirichlet-type BC with a phase shift of $\varphi = -\pi/2$. Setting an uniform pressure amplitude p_a yields the time-dependent pressure BC for a planar wave

$$p(t) = p_a \cos\left(\omega t - \frac{\pi}{2}\right) = p_a \sin(\omega t) \quad (8)$$

where $\omega = 2\pi f$. The other boundary conditions are Neumann-type described by

$$\boldsymbol{n}_\Omega \cdot \boldsymbol{u} = \frac{p}{Z} = \frac{p}{c\rho} \quad (9)$$

where $\boldsymbol{n}_\Omega$ is the inwards normal vector on the boundary. For reflecting boundaries (2) and (4), the acoustic pressure p is zero meaning that the boundary is considered

sound hard. Boundary (2) produces undesired spurious oscillations in the acoustic pressure which falsify the scattered pressure field if not handled properly. One way is to use the *absorbing layers*, equivalent to *perfectly matched layers* to damp oscillations. Another way is to increase the domain size Ω. Here, this circumstance of spurious oscillations is avoided by stopping the simulation as soon as the wavefront approaches the boundary. As the imminent region around the particle is of main interest, effects in the far field are disregarded.

3.3 Simulation structure

To use CWE for scattering phenomena a two-fold approach is proposed.

Study 1 - Plane wave In the first study, the computational domain Ω **without** the sphere is computed. This yields the first solution variables for the acoustic pressure p, which is a time-dependent plane wave propagating along the z-axis.

Study 2 - Distorted wave In the second study, the domain includes the sphere resulting in a pressure field $p2$ which is distorted.

In order to identify the scattered part of the pressure, the plane wave pressure p needs to be subtracted from the distorted wave $p2$ during postprocessing stage. Both studies are carried out with a frequency of $f = 50$ kHz. To avoid reflections from outer boundaries in $\Omega = 100 \times 100$ mm^2 the simulation run begins at $t_{start} = 0$ s and stops at $t_{end} = 100\,\text{mm}/c = 2.915 \times 10^{-4}$ s.

4 Optimal Mesh Size Analysis

Acoustic waves discretized by finite elements should contain a minimum of eight cells per wavelength as popular rule of thumb. However, for acoustic problems using the discontinuous Galerkin discretization scheme different meshing practices apply. To solve the set of equations, Eqs. (5) - (7), the constraints on the meshing parameters are threefold as summarized in Figure 6.

4.1 Meshing considerations

Physical factor

The dG method is intended for acoustic signals that travel a large distance in comparison to the wavelength. Meshing with dG requires as little as two cells per wavelength. A finer mesh may prove counterproductive because there is a compromise between simulation speed and result accuracy. It is supposed that optimal mesh size h is in the range (COMSOL, 2019; Jensen, 2017)

$$\frac{1}{2}\lambda < h < \frac{2}{3}\lambda. \tag{10}$$

As a best practice, it is recommended to build an *User-defined* mesh with minimum element size $\lambda/2$ and maximum cell size $2\lambda/3$. Assuming constant speed of sound

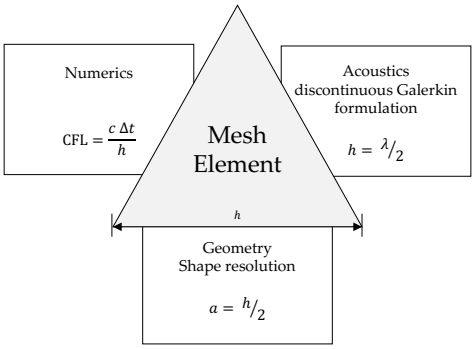

Figure 6. Three factors determine the choice of a suitable mesh for the time-explicit analysis of ultrasound propagation: the CFL number (numerical factor), the discontinuous Galerkin formulation (physical factor) and the resolution of the sphere (geometrical factor).

c the minimum element size scales with the frequency $f = c/\lambda$

$$h \to \mathcal{O}\left((2f)^{-1}\right). \tag{11}$$

Numerical factor

To ensure stability, the time-stepping discretization scheme is strictly coupled to the *Courant-Friedrichs-Lewy* (CFL) condition. The condition restricts the distance a particular information can travel in space within one time-step to achieve convergence and accurate results. For ultrasonic waves a CFL-value of 0.1 is recommended, meaning that within one time-step the wave is allowed to propagate 10% of the given cell size h (COMSOL, 2019). With c being the speed of sound, Δt the time-step size, the CFL-number writes

$$\text{CFL} = \frac{c\Delta t}{h} = 0.1. \tag{12}$$

The minimum time-step required to fulfill the condition can be rewritten in terms of the frequency of the sound-wave,

$$\Delta t = \frac{\text{CFL}\ h}{c} = \frac{\text{CFL}\ \lambda}{2c} = \frac{\text{CFL}}{2f} \tag{13}$$

where the previously recommended relation between acoustic wavelength and minimum cell size $h = \lambda/2$ has been used.

Geometrical factor

The geometrical resolution of small edges is an additional restriction for the minimum mesh element size h. The absolute minimum amount of cell elements to capture the curvature of the sphere boundary is two. Said elements relate with the sphere radius a by

$$a = \frac{h}{\sqrt{2}} = \frac{\lambda}{2\sqrt{2}} \tag{14}$$

where it is assumed that the minimum element size is $h = \lambda/2$.

4.2 Simulation run

Ideally, simulation results ought to be mesh-independent in the sense that the obtained results do not noticeably change with the mesh resolution. A relative change of $< 5\%$ is generally considered acceptable (Versteeg and Malalasekera, 2007). According to Equation (10), the optimal mesh size h is somewhere between $h_{min} = 1/2\lambda$ and $h_{max} = 2/3\lambda$. To verify this best practice, a mesh sensitivity analysis was conducted. The sensitivity analysis was carried out for five different meshes. Figure 7 illustrates the five simulations for $N = 4/6/8/16$, where N represents the number of mesh elements the sphere is resolved by.

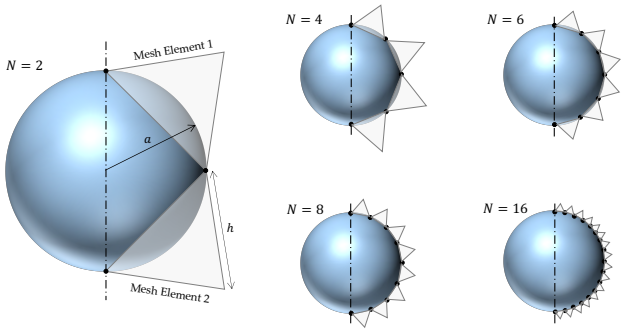

Figure 7. Simulations for the mesh sensitivity analysis.

The five simulations are all conducted using a frequency of $f = 50$ kHz which has a wavelength of $\lambda = 6.86$ mm. Hence, the optimum mesh size for such a simulation is expected to be between $h_{min} = 3.43$ mm and $h_{max} = 4.57$ mm. The size of a single mesh element is given by

$$h = 2\lambda \sin\left(\frac{\pi}{2N}\right) \tag{15}$$

which is valid for a sphere radius $a = \lambda$. Therefore, the theoretical optimum number of nodes is expected between $N_{min} = 4.8$ and $N_{max} = 6.3$. In practice, of course, N is an integer.

5 Results

5.1 Mesh study

The results of the mesh study are summarized in Table 1. To compare the performance of the different simulations the relative error is calculated with reference to the analytical solution. The $N = 4$ case greatly overpredicts the scattered pressure while the $N = 6$ simulation provides the best trade-off between computational time, file size and accuracy. With only two mesh elements per sphere the curvature of the geometry is not adequately discretized which produces spurious oscillations and therefore unphysical results.

The mesh study confirmed that the best practice of setting the mesh size somewhere between $h_{min} = 1/2\lambda$ and $h_{max} = 2/3\lambda$ is confirmed also for scattering phenomena.

5.2 Incident and scattered field

Figure 8 shows the results for the acoustic scattering analysis. On the left side, the incident pressure is plotted which consists of a plane wave propagating at $f = 50$ kHz undisturbed by the particle located at the center of the 2D-axisymmetric setup. In order to visualize the scattered acoustic amplitudes on the right side, the scattered pressure is displayed which is obtained by subtracting the acoustic pressure $p2$ (*i.e.* the driving field) from the acoustic pressure p.

Within the *Pressure Acoustics* interface scattering phenomena can be conveniently modelled by using a background flow field domain node. Here, it is shown that the same phenomena can be modelled using dG and CWE with some minor workarounds.

5.3 Analytical verification

Figure 9 compares the analytical solution for the scattered pressure according to Equation (4) to the numerically computed solution. The results show perfect agreement which means that the modeling approach described in this study is verified. The mesh element size for this chosen according to the modeling guideline for CWE, $h_{min} = \lambda/2 = 3.43$ mm and $h_{max} = \lambda/1.5 = 4.57$ mm.

5.4 Discussion

The discontinuous Galerkin method is characterized by an advantageous discretization scheme, which allows the calculation of ultrasonic wave propagation. Due to meshing restrictions, numerical studies can only be conducted for spheres the size of which is comparable to the wavelength. The solution presented here is in good agreement with the analytical solution, which proves that CWE is a suitable interface for modeling scattering phenomena. In combination with the analytical model, the applicability of the approach can be extended for a wider range of sphere sizes.

The mesh study reveals the sweet spot of accuracy and computational time confirming the suggested mesh size to wavelength ratio.

6 Conclusion

This study investigates the rigid sphere scattering problem by using analytical and numerical approaches.Here, a rigid sphere is hit by an ultrasonic plane wave at a frequency of $f = 50$ kHz in air. The novely of this numerical analysis is the use of the *Convected Wave Equation, Time Explicit* (CWE) interface in COMSOL Multiphysics^{TM} to model scattering phenomena. Note that, the interface was developed primarily for the modeling of the propagation of ultrasonic waves. The results for the scattered pressure are analytically verified. Additionally, a mesh study confirms the particularities of meshing with the discontinuous Galerkin (dG) method.

Table 1. Comparison of the mesh study results. The relative error of the $N = 2$ study is not evaluated since unphysical results are produced.

Number of mesh elements on boundary N [−]	Single element size $h = 2\lambda \sin\left(\frac{\pi}{2N}\right)$ [mm]	Wavelength to element ratio λ/h [−]	Total number of elements [−]	Computational time Δt	File size [GB]	Relative error [%]
2	9.71	0.71	354	1 min 02 s	0.30	n/a
4	5.25	1.33	1016	1 min 27 s	0.85	22.2
6	3.55	1.93	2124	3 min 31 s	1.76	1.9
8	2.67	2.56	3791	4 min 34 s	3.12	3.6
16	1.34	5.10	14552	26 min 38 s	11.97	1.6

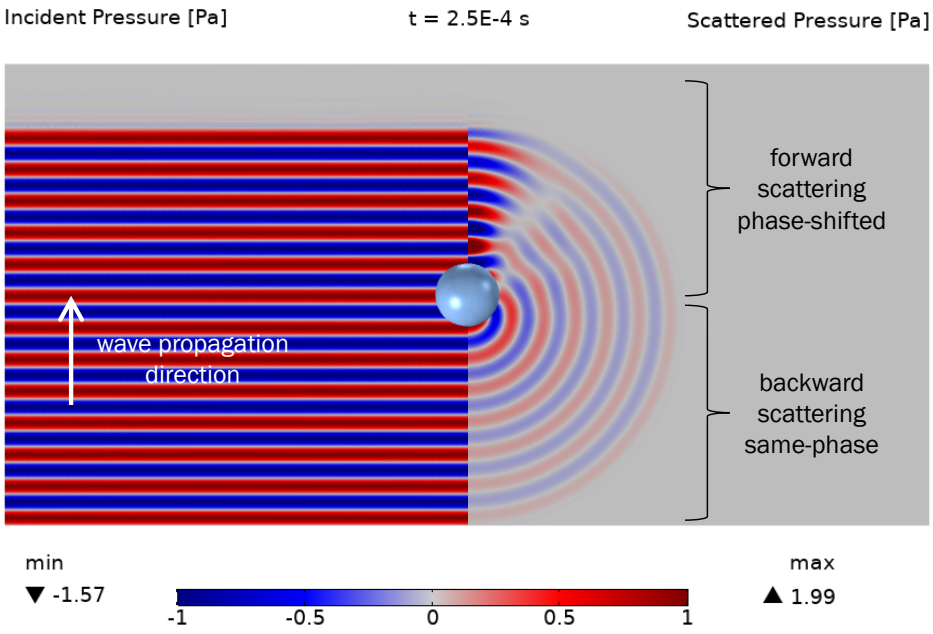

Figure 8. Result of the acoustic scattering analysis. The incident and scattered pressure fields are displayed on the left and right hand side of the graph, respectively.

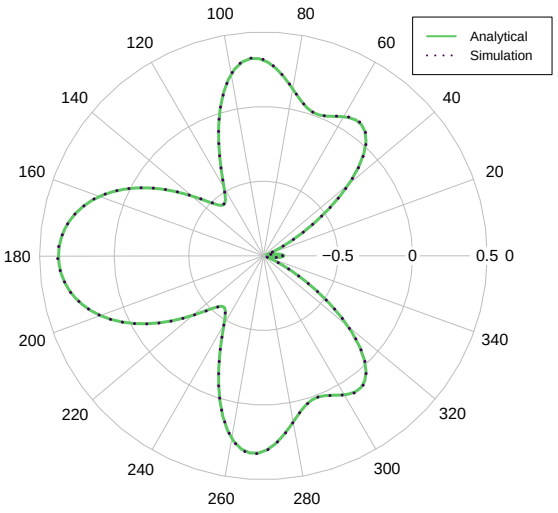

Figure 9. Comparison of the scattered field amplitudes obtained from the analytical and numerical models (gren straight and black dotted lines, respectively).

Because of its memory-efficient way of solving the wave equation the dG method is an optimal tool to study a wide range of phenomena in the field of Ultrasonics, including scientific as well as industrially relevant problems. This simple test-case study provides the fundamentals to pursue advanced numerical work including dissipative effects for ultrasonic waves in air.

References

John A Adam. *Rays, Waves, and Scattering: Topics in Classical Mathematical Physics*, volume 56. Princeton University Press, 2017.

COMSOL. *Acoustics Module User Guide*. COMSOL Multiphysics® v5.4, Stockholm, Sweden, 2019.

Frank Ihlenburg. *Finite element analysis of acoustic scattering*, volume 132. Springer Science & Business Media, 2006.

Mads Herring Jensen. Using the discontinuous galerkin method to model linear ultrasound, 2017.

Donato Rubinetti and Daniel A. Weiss. Acoustically triggered harvesting of nanometer airborne particles–a numerical model for the ultrasonic manipulation. *International Journal of Multiphysics*, 12(4), 2018a. doi:10.21152/1750-9548.12.4.413.

Donato Rubinetti and Daniel A. Weiss. Ultrasound-driven fluid motion-modelling approach. *International Journal of Multiphysics*, 12(1), 2018b. doi:10.21152/1750-9548.12.1.1.

Henk Kaarle Versteeg and Weeratunge Malalasekera. *An introduction to computational fluid dynamics: the finite volume method*. Pearson education, 2007.

Robert Weser, Sebastian Wöckel, Benno Wessely, and Ulrike Hempel. Particle characterisation in highly concentrated dispersions using ultrasonic backscattering method. *Ultrasonics*, 53(3):706–716, 2013. doi:10.1016/j.ultras.2012.10.013.

Robert Weser, Sebastian Woeckel, Benno Wessely, Ulrike Steinmann, Frank Babick, and Michael Stintz. Ultrasonic backscattering method for in-situ characterisation of concentrated dispersions. *Powder technology*, 268:177–190, 2014. doi:10.1016/j.powtec.2014.08.026.